

Analysis of quasi-elastic neutrino charged-current scattering off ^{16}O and neutrino energy reconstruction

A. V. Butkevich

*Institute for Nuclear Research, Russian Academy of Sciences,
60th October Anniversary Prosp. 7A, Moscow 117312, Russia*

(Dated: April 28, 2008)

The charged-current quasi-elastic scattering of muon neutrino on the oxygen target is analyzed for neutrino energy up to 2.5 GeV using the Relativistic Distorted-Wave Impulse Approximation (RDWIA). The inclusive cross sections $d^2\sigma/dQ^2$, calculated within the RDWIA, are lower than the Relativistic Fermi Gas Model (RFGM) results in the range of the square of four-momentum transfer $Q^2 \leq 0.2 \text{ (GeV/c)}^2$. We have also studied the nuclear-model dependence of the neutrino energy reconstruction accuracy using the charged-current quasi-elastic events with no detector effects and background. We found that for one-track events the accuracy is nuclear-model dependent for neutrino energy up to 2.5 GeV.

PACS numbers: 25.30.-c, 25.30.Pt, 13.15.+g

I. INTRODUCTION

The field of neutrino oscillations is rapidly developing. The goals of the current and planned set of accelerator-based neutrino experiments [1–7] are the precision measurements of observed neutrino mass splitting and the detailed study of the neutrino mixing matrix. The data of these experiments will greatly extend the statistics due to extremely intense neutrino beamline.

To study the neutrino oscillation effects on the terrestrial distance scale, the neutrino beams cover the energy range from a few hundred MeV to several GeV. In this energy range, the dominant contribution to the neutrino-nucleus cross section comes from the charged-current (CC) quasi-elastic (QE) reactions and resonance production processes. The cross section data in this energy range are rather scarce and were taken on the targets, which are not used in the neutrino oscillation experiments (i.e. water, iron, lead or plastic).

In this situation, the statistical uncertainties should be negligible as compared to systematic errors in the incident neutrino flux, neutrino interaction model and the detector effects on the neutrino events selection and neutrino energy reconstruction. Apparently, these uncertainties produce systematic errors in the extraction of oscillation parameters.

To evaluate the neutrino mass squared difference in the muon neutrino disappearance exper-

iments, the probability of ν_μ disappearance versus neutrino energy is measured. Because the CCQE interaction represents a two-particle scattering process, it forms a good signal sample, and the neutrino energy may be estimated using the kinematics of this reaction. There are two ways of measuring the neutrino energy: either kinematic or calorimetric reconstruction. In detectors with the energy threshold for proton detection $\varepsilon_{th}^p \geq 1$ GeV (Cherenkov detectors) the muon neutrino CCQE interactions will produce the one-track events, i.e. only muons are detected in the final states. The kinematic reconstruction is applied for these events. Assuming the target nucleon to be at rest inside the nucleus, the correlation between the incident neutrino energy and a reconstructed muon momentum and scattering angle is used in this method.

In the fine-grained detectors the two-track CCQE events are detected, and the calorimetric reconstruction can be applied, if the particle identification of the second track and the resolution for proton momentum are reliable. In this case the visible neutrino energy is simply a sum of the reconstructed muon energy and kinematic proton energy. In this paper we consider the procedures for neutrino energy reconstruction, which are based on the kinematics of the CCQE interaction.

In general, the detector efficiency and energy response are highly dependent on the type of interaction: QE or non-QE (the resonance and deep inelastic scattering). The Monte Carlo (MC) simulation of the detector response to neutrino interactions is used for tuning the values of cuts for separation of the QE and non-QE (nQE) events and for estimating the efficiency of detecting the CCQE events after all cuts. To model the scattering from a nuclei, the most part of an event generator [8] is based on the RFGM [9], in which the nucleus is described as a system of quasi-free nuclei with a flat nucleon momentum distribution up to the same Fermi momentum p_F and nuclear binding energy ϵ_b . But this model does not take into account the nuclear shell structure, the final state interaction (FSI) between the outgoing nucleon and residual nucleus and the presence of short-range nucleon-nucleon (NN) correlations, leading to appearance of a high-momentum and high-energy component in the nucleon momentum-energy distribution in the target.

The comparison with the high-precision electron scattering data has shown [10] that the accuracy of the RFGM prediction becomes poor at low Q^2 , where the nuclear effects are largest, and this model fails [13] in application to exclusive cross sections. The modern quasi-elastic neutrino scattering data (the CCQE event distribution as a function of Q^2) [2, 11, 12] also reveal the inadequacies in the present neutrino cross section simulation. The data/MC disagreement shows the data deficit in the low Q^2 region ($Q^2 \leq 0.2$ GeV²) and the data excess in the high Q^2 region. The disagreement at low Q^2 would eventually result in the data/MC disagreement in the reconstructed neutrino energy.

The Relativistic Distorted-Wave Impulse Approximation, which takes into account the nuclear shell structure and FSI effects, was developed for description of electron-nucleus scattering, and it was successfully tested against the data [14]. The RDWIA approach was also applied to neutrino-nucleus (νA) interactions for calculating the exclusive and inclusive QE cross sections [13, 15–17]. In Ref. [13] the FSI effects on the inclusive cross section in the presence of the NN-correlations were estimated.

The aim of this work is twofold. First, we compute the RDWIA CCQE cross section versus Q^2 for muon neutrino scattering off oxygen. Second, we show the nuclear-model dependence of the efficiency of two-track CCQE events selection. We also estimate systematic uncertainties in the reconstructed neutrino energy within the RDWIA and RFGM taking into account the nucleon momentum distribution in the target, i.e. the nucleon Fermi motion effect.

The outline of this paper is as follows. In Sec. II we present briefly the formalism for CCQE scattering process and the RDWIA model. The nuclear-model dependence of cuts, which are applied for CCQE events selection, as well as the neutrino energy reconstruction methods are discussed in Sec. III. The results of numerical calculations are presented in Sec. IV. Our conclusions are summarized in Sec. V. In Appendix A we present the equation for neutrino energy, and in Appendix B the expressions for the moments of the reconstructed neutrino energy distribution are given.

II. FORMALISM OF QUASI-ELASTIC SCATTERING AND MODELS

We consider the electron and neutrino charged-current QE exclusive

$$\nu(k_i) + A(p_A) \rightarrow l(k_f) + N(p_x) + B(p_B), \quad (1)$$

and inclusive

$$\nu(k_i) + A(p_A) \rightarrow l(k_f) + X \quad (2)$$

scattering-off nuclei in the one-W-boson exchange approximation. Here l represents the scattered lepton (electron or muon), $k_i = (\varepsilon_i, \mathbf{k}_i)$ and $k_f = (\varepsilon_f, \mathbf{k}_f)$ are the initial and final lepton momenta, $p_A = (\varepsilon_A, \mathbf{p}_A)$, and $p_B = (\varepsilon_B, \mathbf{p}_B)$ are the initial and final target momenta, $p_x = (\varepsilon_x, \mathbf{p}_x)$ is the ejectile nucleon momentum, $q = (\omega, \mathbf{q})$ is the momentum transfer carried by the virtual W-boson, and $Q^2 = -q^2 = \mathbf{q}^2 - \omega^2$ is the W-boson virtuality.

A. CCQE neutrino-nucleus cross sections

In the laboratory frame the differential cross section for the exclusive (anti)neutrino CCQE reaction, in which only a single discrete state or narrow resonance of the target is excited, can be written as

$$\frac{d^5\sigma}{d\varepsilon_f d\Omega_f d\Omega_x} = R \frac{|\mathbf{p}_x| \varepsilon_x |\mathbf{k}_f|}{(2\pi)^5 \varepsilon_i} \frac{G^2 \cos^2 \theta_c}{2} L_{\mu\nu} W^{\mu\nu}, \quad (3)$$

where Ω_f is the solid angle for the lepton momentum, Ω_x is the solid angle for the ejectile nucleon momentum, $G \simeq 1.16639 \times 10^{-11} \text{ MeV}^{-2}$ is the Fermi constant, θ_C is the Cabbibo angle ($\cos \theta_C \approx 0.9749$), $L_{\mu\nu}$ and $W^{\mu\nu}$ are, respectively, the lepton and weak CC nuclear tensors. The recoil factor R is given by

$$R = \int d\varepsilon_x \delta(\varepsilon_x + \varepsilon_B - \omega - m_A) = \left| 1 - \frac{\varepsilon_x}{\varepsilon_B} \frac{\mathbf{p}_x \cdot \mathbf{p}_B}{\mathbf{p}_x \cdot \mathbf{p}_x} \right|^{-1}, \quad (4)$$

and ε_x is the solution to the equation

$$\varepsilon_x + \varepsilon_B - m_A - \omega = 0, \quad (5)$$

where $\varepsilon_B = \sqrt{m_B^2 + \mathbf{p}_B^2}$, $\mathbf{p}_B = \mathbf{q} - \mathbf{p}_x$, $\mathbf{p}_x = \sqrt{\varepsilon_x^2 - m^2}$, and m_A , m_B , and m are masses of the target, recoil nucleus and nucleon, respectively. The missing momentum p_m and missing energy ε_m are defined by

$$\mathbf{p}_m = \mathbf{p}_x - \mathbf{q} \quad (6a)$$

$$\varepsilon_m = m + m_B - m_A \quad (6b)$$

The lepton tensor can be written as a sum of symmetric $L_S^{\mu\nu}$ and antisymmetric $L_A^{\mu\nu}$ tensors

$$L^{\mu\nu} = L_S^{\mu\nu} + L_A^{\mu\nu} \quad (7a)$$

$$L_S^{\mu\nu} = 2 \left(k_i^\mu k_f^\nu + k_i^\nu k_f^\mu - g^{\mu\nu} k_i \cdot k_f \right) \quad (7b)$$

$$L_A^{\mu\nu} = h 2i \epsilon^{\mu\nu\alpha\beta} (k_i)_\alpha (k_f)_\beta, \quad (7c)$$

where h is $+1$ for a positive lepton helicity, and -1 for a negative lepton helicity, $\epsilon^{\mu\nu\alpha\beta}$ is the antisymmetric tensor with $\epsilon^{0123} = -\epsilon_{0123} = 1$. The weak CC hadronic tensors $W_{\mu\nu}$ are given by bilinear products of the transition matrix elements of the nuclear CC operator J_μ between the initial nucleus state $|A\rangle$ and the final state $|B_f\rangle$ as

$$W_{\mu\nu} = \sum_f \langle B_f, p_x | J_\mu | A \rangle \langle A | J_\nu^\dagger | B_f, p_x \rangle, \quad (8)$$

where the sum is taken over undetected states.

In the inclusive reactions (2) only the outgoing lepton is detected, and the differential cross sections can be written as

$$\frac{d^3\sigma}{d\varepsilon_f d\Omega_f} = \frac{1}{(2\pi)^2} \frac{|\mathbf{k}_f|}{\varepsilon_i} \frac{G^2 \cos^2 \theta_c}{2} L_{\mu\nu} \mathcal{W}^{\mu\nu}, \quad (9)$$

where $\mathcal{W}^{\mu\nu}$ is an inclusive hadronic tensor. In the reference frame, in which the z axis is parallel to the momentum transfer $\mathbf{q} = \mathbf{k}_i - \mathbf{k}_f$ and the y axis is parallel to $\mathbf{k}_i \times \mathbf{k}_f$, the exclusive neutrino scattering cross sections take the forms

$$\begin{aligned} \frac{d^5\sigma}{d\varepsilon_f d\Omega_f d\Omega_x} = & \frac{|\mathbf{p}_x| \varepsilon_x}{(2\pi)^5} G^2 \cos^2 \theta_c \varepsilon_f |\mathbf{k}_f| R \{ v_0 R_0 + v_T R_T + v_{TT} R_{TT} \cos 2\phi + v_{zz} R_{zz} \\ & + (v_{xz} R_{xz} - v_{0x} R_{0x}) \cos \phi - v_{0z} R_{0z} + h [v_{yz} (R'_{yz} \sin \phi + R_{yz} \cos \phi) \\ & - v_{0y} (R'_{0y} \sin \phi + R_{0y} \cos \phi) - v_{xy} R_{xy}] \}, \end{aligned} \quad (10)$$

where θ, φ are lepton scattering angles, and θ_x, ϕ are outgoing nucleon angles, v_i are the neutrino coupling coefficients, and R_i are independent response functions [13], which depend on the variables $Q^2, \omega, |\mathbf{p}_x|$, and θ_x . Similarly, the inclusive lepton scattering cross sections are reduced to

$$\frac{d^3\sigma}{d\varepsilon_f d\Omega_f} = \frac{G^2 \cos^2 \theta_c}{(2\pi)^2} \varepsilon_f |\mathbf{k}_f| (v_0 R_0 + v_T R_T + v_{zz} R_{zz} - v_{0z} R_{0z} - h v_{xy} R_{xy}) \quad (11)$$

where the response functions now depend on Q^2 and ω only [13].

We describe the lepton-nucleon scattering in the Impulse Approximation (IA), in which only one nucleon of the target is involved in the reaction, and the nuclear current is written as a sum of single-nucleon currents. Then, the nuclear matrix element in Eq.(8) takes the form

$$\langle p, B | J^\mu | A \rangle = \int d^3r \exp(i\mathbf{t} \cdot \mathbf{r}) \bar{\Psi}^{(-)}(\mathbf{p}, \mathbf{r}) \Gamma^\mu \Phi(\mathbf{r}), \quad (12)$$

where Γ^μ is the vertex function, $\mathbf{t} = \varepsilon_B \mathbf{q} / W$ is the recoil-corrected momentum transfer, $W = \sqrt{(m_A + \omega)^2 - \mathbf{q}^2}$ is the invariant mass, Φ and $\Psi^{(-)}$ are relativistic bound-state and outgoing wave functions.

The single-nucleon charged current has $V-A$ structure $J^\mu = J_V^\mu + J_A^\mu$. For the free-nucleon vertex function $\Gamma^\mu = \Gamma_V^\mu + \Gamma_A^\mu$ we use the CC2 vector current vertex function [18]

$$\Gamma_V^\mu = F_V(Q^2) \gamma^\mu + i \sigma^{\mu\nu} \frac{q_\nu}{2m} F_M(Q^2) \quad (13)$$

and the axial current vertex function

$$\Gamma_A^\mu = F_A(Q^2) \gamma^\mu \gamma_5 + P(Q^2) q^\mu \gamma_5, \quad (14)$$

where $\sigma^{\mu\nu} = i[\gamma^\mu, \gamma^\nu]/2$. The weak vector form factors F_V and F_M are related with corresponding electromagnetic factors for proton $F_{i,p}^{(el)}$ and neutron $F_{i,n}^{(el)}$ by the hypothesis of conserved vector current (CVC)

$$F_i = F_{i,p}^{(el)} - F_{i,n}^{(el)}, \quad (15)$$

where $F_V^{(el)}$ and $F_M^{(el)}$ are the Dirac and Pauli nucleon form factors. We use the approximation of [19] for these form factors. Because the bound nucleons are off shell, we employ the de Forest prescription for off-shell vertex [18] and the Coulomb gauge - for vector current J_V .

The axial F_A and pseudoscalar F_P form factors in the dipole approximation are parameterized as

$$F_A(Q^2) = \frac{F_A(0)}{(1 + Q^2/M_A^2)^2}, \quad F_P(Q^2) = \frac{2mF_A(Q^2)}{m_\pi^2 + Q^2}, \quad (16)$$

where $F_A(0) = 1.267$, $M_A \simeq 1.032$ GeV is the axial mass, and m_π is the pion mass

B. Models

In the independent particle shell model the relativistic bound-state functions Φ in Eq.(12) are obtained within the Hartree–Bogoliubov approximation in the $\sigma - \omega$ model [20]. The bound-state spinor takes the form

$$\Phi_{\kappa m}(\mathbf{r}) = \begin{pmatrix} F_\kappa(r) \mathcal{Y}_{\kappa m}(\hat{r}) \\ iG_{-\kappa}(r) \mathcal{Y}_{-\kappa m}(\hat{r}) \end{pmatrix}, \quad (17)$$

where

$$\mathcal{Y}_{\kappa m}(\hat{r}) = \sum_{\nu, m_s} \left\langle \begin{matrix} \ell & \frac{1}{2} \\ \nu & m_s \end{matrix} \middle| \begin{matrix} j \\ m \end{matrix} \right\rangle Y_{\ell\nu}(\hat{r}) \chi_{m_s} \quad (18)$$

is the spin spherical harmonic, and the orbital and total angular momenta are given, respectively, by

$$\ell = S_\kappa(\kappa + \frac{1}{2}) - \frac{1}{2} \quad (19a)$$

$$j = S_\kappa\kappa - \frac{1}{2} \quad (19b)$$

with $S_\kappa = \text{sign}(\kappa)$. The missing momentum distribution is then

$$P(p_m) = \frac{S_\alpha}{2\pi^2} \left(|\tilde{F}_\kappa(p_m)|^2 + |\tilde{G}_\kappa(p_m)|^2 \right), \quad (20)$$

where

$$\tilde{F}_\kappa(p) = \int dr r^2 j_\ell(p_m r) F_\kappa(r) \quad (21a)$$

$$\tilde{G}_{-\kappa}(p) = \int dr r^2 j_{\ell'}(p_m r) G_{-\kappa}(r), \quad (21b)$$

and $j_\ell(x)$ is the Bessel function of order ℓ , and $\ell' = 2j - \ell$. In this work the bound-nucleon wave functions [21] are used in the numerical analysis with the normalization factors S_α relative to full occupancy of ^{16}O : $S(1p_{3/2}) = 0.66$, $S(1p_{1/2}) = 0.7$ [14] and $S(1s_{1/2}) = 1$. Note that the calculation of the bound-nucleon wave function for $1p_{3/2}$ -state includes the incoherent contribution of the unresolved $2s_{1/2}d_{5/2}$ doublet [22].

In the RDWIA the ejectile wave function Ψ in Eq.(12) is obtained following the direct Pauli reduction method [23, 24]. It is well known that the Dirac spinor

$$\Psi = \begin{pmatrix} \Psi_+ \\ \Psi_- \end{pmatrix} \quad (22)$$

can be written in terms of its positive energy component Ψ_+ as

$$\Psi = \begin{pmatrix} \Psi_+ \\ \frac{\boldsymbol{\sigma} \cdot \mathbf{p}}{E + M + S - V} \Psi_+ \end{pmatrix} \quad (23)$$

where $S = S(r)$ and $V = V(r)$ are the scalar and vector potentials for the nucleon with energy E . The upper component Ψ_+ can be related to the Schrödinger-like wave function ξ by the Darwin factor $D(r)$, i.e.

$$\Psi_+ = \sqrt{D(r)} \xi, \quad (24)$$

$$D(r) = \frac{E + M + S(r) - V(r)}{E + M}. \quad (25)$$

The two-component wave function ξ is the solution of the Schrödinger equation containing equivalent central and spin-orbit potentials, which are functions of the scalar and vector potentials S and V , and are energy dependent. We use the LEA program [25] for numerical calculation of the distorted wave functions with EDAD1 SV relativistic optical potential [26].

In the Plane-Wave Impulse Approximation (PWIA) the final state interaction between the outgoing nucleon and the residual nucleus is neglected, and the nonrelativistic PWIA exclusive cross section has a factorized form [27]

$$\frac{d^5\sigma}{d\varepsilon_f d\Omega_f d\Omega_x} = K \sigma_{ex} \mathcal{P}(E, \mathbf{p}) \quad (26)$$

where $K = Rp_x \varepsilon_x / (2\pi)^5$ is the phase-space factor and σ_{ex} is the half-off-shell cross section for neutrino scattering by a moving nucleon. The nuclear spectral function $\mathcal{P}(E, \mathbf{p})$ can be written as

$$\mathcal{P}(E, \mathbf{p}) = \sum_f \left| \langle B_f | a(\mathbf{p}) | A \rangle \right|^2 \delta(E - \varepsilon_m) \quad (27)$$

and the nucleon momentum distribution $P_\beta(\mathbf{p})$ for the orbit β is related to the upper component of the corresponding bound-state wave function (21a) as

$$P_\beta(\mathbf{p}) = \frac{S_\beta}{2\pi^2} \left| \tilde{F}_\beta(\mathbf{p}) \right|^2. \quad (28)$$

According to the JLab data [14], the occupancy of the independent particle shell model orbitals of ^{16}O equals about 75%, on the average. In this work we assume that the missing strength (25%) can be attributed to the short-range NN-correlations in the ground state, leading to appearance of high-momentum and high-energy nucleon distribution in the target. In order to estimate this effect in the inclusive cross sections, we consider the phenomenological model [28, 29] where the high-momentum (HM) part of the spectral function is determined by excited states with one or more nuclei in a continuum.

In our calculations of the inclusive cross sections only the real part of the optical potential is included, because the complex potential produces absorptions of flux. Then, the contribution of the $1p$ - and $1s$ -states to the inclusive cross section $(d^3\sigma/d\varepsilon_f d\Omega_f)_{RDWIA}$ can be obtained by integrating the exclusive cross sections (10) over Ω_x . The effect of the FSI on the inclusive cross section can be evaluated using the ratio

$$\Lambda(\varepsilon_f, \Omega_f) = \left(\frac{d^3\sigma}{d\varepsilon_f d\Omega_f} \right)_{RDWIA} / \left(\frac{d^3\sigma}{d\varepsilon_f d\Omega_f} \right)_{PWIA}, \quad (29)$$

where $(d^3\sigma/d\varepsilon_f d\Omega_f)_{PWIA}$ is the result obtained in the PWIA. Then the total inclusive cross section can be written as

$$\frac{d^3\sigma}{d\varepsilon_f d\Omega_f} = \left(\frac{d^3\sigma}{d\varepsilon_f d\Omega_f} \right)_{RDWIA} + \Lambda(\varepsilon_f, \Omega_f) \left(\frac{d^3\sigma}{d\varepsilon_f d\Omega_f} \right)_{HM}, \quad (30)$$

where $(d^3\sigma/d\varepsilon_f d\Omega_f)_{HM}$ is the high-momentum component contribution into the inclusive cross section [13].

III. ANALYSIS OF CCQE INTERACTION AND NEUTRINO ENERGY RECONSTRUCTION

A. Differential cross sections $d\sigma/d\cos\theta$ and $d\sigma/dQ^2$

The charged-current QE events distributions as a function of Q^2 or $\cos\theta$ were measured by K2K [11] and MiniBoone [2, 12] experiments. High statistic data show a disagreement with the RFGM prediction. The data samples exhibit significant deficit in the region of low $Q^2 \leq 0.2 \text{ GeV}^2$ and small muon scattering angles, which corresponds to forward-going muons. In Refs. [2, 12] it was shown that the data/MC disagreement is not due to mis-modeling of the incoming neutrino energy spectrum, but due to inaccuracy in the simulation of CCQE interactions. To tune the Fermi gas model to the low Q^2 region, an additional parameter was introduced, which reduced the phase volume of the nucleon Fermi gas at low momentum transfer. In the region of high Q^2 the data excess is observed, and the values of the axial vector mass M_A , obtained from a fit to the measured data, are higher, than the results of previous experiments.

We calculated the differential cross sections $d\sigma/d\cos\theta$ and $d^2\sigma/dQ^2$ for neutrino CCQE scattering off oxygen target in the RDWIA, PWIA and RFGM approaches.

We note that in the case of (anti)neutrino scattering off free nucleon CCQE the differential cross sections [30] $d\sigma^{\nu,\bar{\nu}}/dQ^2$ at $Q^2 \rightarrow 0$ can be written as

$$\frac{d\sigma^{\nu,\bar{\nu}}}{dQ^2} = \frac{G^2}{2\pi} \cos^2\theta_c [F_V^2(0) + F_A^2(0)] \quad (31)$$

and do not depend on the neutrino energy. The difference

$$\frac{d\sigma^\nu}{dQ^2} - \frac{d\sigma^{\bar{\nu}}}{dQ^2} = \frac{G^2}{\pi} \cos^2\theta_c \frac{Q^2}{m\varepsilon_i} \left(1 - \frac{Q^2}{4m\varepsilon_i}\right) (F_V + F_M)F_A \quad (32)$$

is proportional to F_A and decreases with neutrino energy. In the range of $\varepsilon_i \sim 0.5 \div 1 \text{ GeV}$ it can be used for measuring the axial form factor F_A .

B. Selection of charged-current QE two-track events

At the first step, the CC candidate events are selected by requiring that at least one reconstructed track must be long and corresponding to a minimum ionizing particle with the momentum higher, than a few hundred MeVs. The background is originated by neutral-current (NC) interactions producing a charged pion.

In the CC event candidates, the events with one or two reconstructed tracks, with vertex in the active target are selected like the CCQE events. No other tracks are allowed to be connected

with this event vertex. The two-track events are divided into two samples: QE and nQE enriched samples. Depending on detector capabilities dE/dx , the information is applied to the second track for π/p separation [31]. Since the QE interaction is a two-particle scattering process, the measurement of the muon momentum and angle allows predicting the angle of a recoil proton (the second track) assuming the neutrino scattering off to occur with a nucleon at rest. If the measured second track agrees with this prediction within $\Delta\theta$, it represents likely the CCQE event. Using the MC simulation based on the Fermi gas model, the values of $\Delta\theta$ are chosen to give a reliable separation between the QE and nQE events.

To study the nuclear-model dependence of this cut, we consider the angle θ_{pq} between the direction of outgoing proton and momentum transfer. For neutrino QE scattering off, the nucleon is at rest $\mathbf{q} = \mathbf{p}_x$ and $\cos\theta_{pq}=1$. For scattering off bound nucleon with momentum \mathbf{p}_m , it follows from Eq.(6a), that

$$\cos\theta_{pq} = \frac{\mathbf{p}_x^2 + \mathbf{q}^2 - \mathbf{p}_m^2}{2|\mathbf{p}_x||\mathbf{q}|}. \quad (33)$$

The maximum value of θ_{pq} corresponds to scattering off nucleon with a maximum momentum \mathbf{p}_{max} , i.e.

$$\cos\theta_{pq}^m = \frac{\mathbf{p}_x^2 + \mathbf{q}^2 - \mathbf{p}_{max}^2}{2|\mathbf{p}_x||\mathbf{q}|} \quad (34)$$

and $\cos\theta_{pq}^m \leq \cos\theta_{pq} \leq 1$.

In the RFGM the recoil proton energy $\varepsilon_x = \sqrt{\mathbf{p}_m^2 + m^2} - \epsilon_b + \omega$ and for $|\mathbf{p}_{max}| = p_F$ we have

$$\mathbf{p}_x^2 = p_F^2 + \tilde{\omega}^2 + 2\tilde{\omega}\sqrt{p_F^2 + m^2}, \quad (35)$$

where $\tilde{\omega} = \omega - \epsilon_b$. In the RDWIA the energy and momentum of an outgoing nucleon can be written (see Eqs.(5), (6a)) as follow:

$$\mathbf{p}_x = \mathbf{p}_m + \mathbf{q} \quad (36a)$$

$$\varepsilon_x = \omega + m_A - \varepsilon_B. \quad (36b)$$

For the scattering off shell nucleon with a maximum momentum \mathbf{p}_{max} the energy of recoil nuclei is

$$\varepsilon_B = \sqrt{\mathbf{p}_{max}^2 + m_B^2} \approx m_B + \mathbf{p}_{max}^2/2m_B, \quad (37)$$

where $m_B = m_A - m + \varepsilon_m$. In the numerical calculations we use $|\mathbf{p}_{max}|=500$ MeV/c and the mean missing energy $\langle\varepsilon_m\rangle=27.1$ MeV for the oxygen target. Using Eqs.(34), (36a), (36b), and (37), we have

$$\cos\theta_{pq}^m = \frac{\tilde{\omega}(2m + \tilde{\omega}) + (Q^2 - m^2) - \mathbf{p}_{max}^2}{2\sqrt{\tilde{\omega}(2m + \tilde{\omega})}(Q^2 + m^2)}, \quad (38)$$

where $\bar{\omega} = \omega - \langle \varepsilon_m \rangle - \mathbf{p}_{max}^2 / 2m_B^*$ and $m_B^* = m_A - m + \langle \varepsilon_m \rangle$. It follows from (34), that in the RDWIA the phase volume in $(\cos \theta_{pq}, Q^2)$ coordinates is larger, than in the Fermi gas model, and this difference decreases with momentum transfer.

C. Reconstruction of neutrino energy

In the kinematic reconstruction the neutrino energy ε_r is formed assuming the target nucleon to be at rest inside a nucleus

$$\varepsilon_r = \frac{\varepsilon_f(m - \epsilon_b) - (\epsilon_b^2 - 2m\epsilon_b + m_\mu^2)/2}{(m - \epsilon_b) - \varepsilon_f + k_f \cos \theta}. \quad (39)$$

This formula ignores the nucleon momentum distribution for the event reconstruction. Using Eq.(36a) and the energy balance in the RFGM

$$\varepsilon_i + \sqrt{\mathbf{p}_m^2 + m^2} - \epsilon_b = \varepsilon_f + \varepsilon_x, \quad (40)$$

or

$$\varepsilon_i + m_A = \varepsilon_x + \varepsilon_f + \varepsilon_B. \quad (41)$$

in the RDWIA for shell nucleon and

$$\varepsilon_i + \varepsilon_N = \varepsilon_f + \varepsilon_x. \quad (42)$$

for nucleons with energy ε_N in the correlated NN-pair, we obtain the second-order equation for the neutrino energy, which takes into account the bound nucleon momentum and the energy distributions

$$A\varepsilon_r^2 - B\varepsilon_r + C = 0. \quad (43)$$

The expressions for coefficients A, B , and C are given in Appendix A for the RFGM and RDWIA. The solution of (43)

$$\varepsilon_r = \left(B + \sqrt{B^2 - 4AC} \right) / 2A \quad (44)$$

is the reconstructed neutrino energy, which depends on the variables $|\mathbf{p}_m|$, ε_m , and $\cos \tau = \mathbf{p} \cdot \mathbf{q} / |\mathbf{p} \cdot \mathbf{q}|$. So, the distribution $\varepsilon_r(|\mathbf{p}_m|, \varepsilon_m, \cos \tau)$ corresponds to measured values of $(k_f, \cos \theta)$ and at $\varepsilon_m, \mathbf{p}_m \rightarrow 0$ Eq.(44) has asymptotic form given by Eq.(39).

The n -th moment of $\varepsilon_r(k_f, \cos \theta, \mathbf{p}_m, \varepsilon_m)$ distribution versus k_f and $\cos \theta$ can be written as

$$\langle \varepsilon_r^n(k_f, \cos \theta) \rangle = \int_{p_{min}}^{p_{max}} d\mathbf{p} \int_{\varepsilon_{min}}^{\varepsilon_{max}} S(\mathbf{p}, \varepsilon) [\varepsilon_r(k_f, \cos \theta, \mathbf{p}, \varepsilon)]^n d\varepsilon, \quad (45)$$

where $S(\mathbf{p}, \varepsilon)$ is the probability density function (p.d.f.) for the nucleon momentum and energy, the target nucleon momentum and energy distribution being normalized with respect to the unit area. The mean of $\varepsilon_r(k_f, \cos \theta)$ and its variance $\sigma^2(\varepsilon_r)$ are defined by

$$\bar{\varepsilon}_r(k_f, \cos \theta) = \langle \varepsilon_r(k_f, \cos \theta) \rangle, \quad (46a)$$

$$\sigma^2(\varepsilon_r) = \langle \varepsilon_r^2(k_f, \cos \theta) \rangle - \bar{\varepsilon}_r^2(k_f, \cos \theta) \quad (46b)$$

In principle, the cut $R = \sigma(\varepsilon_r)/\bar{\varepsilon}_r \leq \delta$ may be imposed (event by event) to select the events with well-reconstructed energy.

The accuracy of reconstructed energy $\varepsilon_r(\varepsilon_i)$ as a function of ε_i can be estimated using the moments of $\varepsilon_r(k_f, \cos \theta)$ distribution

$$\langle \varepsilon_r^n(\varepsilon_i) \rangle = \int dk_f \int W(k_f, \cos \theta) [\varepsilon_r(k_f, \cos \theta)]^n d\cos \theta, \quad (47)$$

where $W(k_f, \cos \theta)$ is the p.d.f. of the muon momentum and scattering angle, i.e.

$$W(k_f, \cos \theta) = \frac{1}{\sigma_{tot}(\varepsilon_i)} \frac{d^2\sigma}{dk_f d\cos \theta}, \quad (48)$$

and

$$\sigma_{tot}(\varepsilon_i) = \int \frac{d^2\sigma}{dk_f d\cos \theta} dk_f d\cos \theta. \quad (49)$$

Usually, to select the CC events, k_f and $\cos \theta$ cuts are applied: $k_f \geq k_{cut}$ and $\cos \theta \geq (\cos \theta)_{cut}$. The lower limits of integration in Eq.(47) are $(k_f)_{min} = k_{cut}$, $(\cos \theta)_{min} = (\cos \theta)_{cut}$ and $[\varepsilon_r(k_f, \cos \theta)]^n = \langle \varepsilon^n(k_f, \cos \theta) \rangle$, if the nucleon Fermi motion effect is taken into account, or $\varepsilon_r(k_f, \cos \theta)$ is given by Eq.(39), if this effect is neglected. It's worth to emphasize here, that formula (39) can not be used for neutrino energy reconstruction at $\varepsilon_f \geq (m - \epsilon_b) + k_f \cos \theta$ or $Q^2 = Q_0^2 \geq 2m\varepsilon_i - m_\mu^2$, because the value of resulting ε_r is negative in this region. In terms of energy transfer, it corresponds to the range $\omega_1 \leq \omega \leq \omega_2$, where ω_2 is the solution to the equation

$$Q_0^2 = 2\varepsilon_i(\varepsilon_f - k_f \cos \theta) - m_\mu^2. \quad (50)$$

In the RDWIA, ω_1 is the value of ω , at which

$$Q_0^2 = \left[|\mathbf{p}_{max}| + \sqrt{\tilde{\omega}^2 + 2m\tilde{\omega}} \right]^2 - \omega^2 \quad (51)$$

with $\tilde{\omega} = \omega - \langle \varepsilon_m \rangle - p_{max}^2/2m_B^*$, and in the RFGM, ω_1 is the solution to the equation

$$Q_0^2 = \left[p_F + \sqrt{p_F^2 + 2\varepsilon_F \tilde{\omega} + \tilde{\omega}^2} \right]^2 - \omega^2, \quad (52)$$

where $\tilde{\omega} = \omega - \varepsilon_b$ and $\varepsilon_F^2 = p_F^2 + m^2$. The size of this range $\Delta\omega = \omega_2 - \omega_1$ is proportional to $|\mathbf{p}_{max}|$ (p_F) and reduces with increasing $\cos\theta$.

The reconstructed neutrino energy $\bar{\varepsilon}_r = \langle \varepsilon_r \rangle$ is smeared with variance

$$\sigma^2(\varepsilon_i) = \langle \varepsilon_r^2(\varepsilon_i) \rangle - \bar{\varepsilon}_r^2(\varepsilon_i) \quad (53)$$

and biased with

$$\Delta(\varepsilon_i) = \varepsilon_i - \bar{\varepsilon}_r \quad (54)$$

Using this mean energy approach, we estimated the accuracy of the neutrino energy reconstruction with and without the nucleon Fermi motion effect in the RDWIA and RFGM approaches. The expressions for the moments $\langle \varepsilon_r^n(k_f, \cos\theta) \rangle$ and $\langle \varepsilon_r^n(\varepsilon_i) \rangle$ are given in Appendix B.

In the calorimetric reconstruction ε_r is formed as a sum of muon energy ε_f , kinematic proton energy T_p and the mean missing energy $\langle \varepsilon_m \rangle$

$$\varepsilon(k_f, \cos\theta) = \varepsilon_f + T_p + \langle \varepsilon_m \rangle. \quad (55)$$

The expressions for the moments of $\varepsilon_r(k_f, \cos\theta)$ distribution are given in Appendix B. However, the neutrino energy is underestimated in the kinematical and calorimetric reconstructions, when the event represents, in fact, the nQE event, but looks like the QE event.

IV. RESULTS

The resulting fluxes of neutrino are predicted with the mean energy of ~ 0.7 GeV in the Mini-BooNE and T2K experiments, and ~ 2.5 GeV at the MINOS and MINERvA detectors. We calculated the differential inclusive cross sections $d^3\sigma/d\omega dQ^2$ and $d^2\sigma/d\omega d\cos\theta$ of CCQE ν_μ scattering off ^{16}O for these energies using the LEA code, which was adopted for neutrino interaction [13]. In Fig.1 $d^3\sigma/d\omega dQ^2$ cross sections, calculated within the RDWIA, PWIA, and RFGM, are shown for the neutrino energy $\varepsilon_\nu=0.7$ GeV, and in Fig.2 for $\varepsilon_\nu=2.5$ GeV as a function of Q^2 . Also shown in Figures 1 and 2 show the high-momentum component contributions of the nucleon momentum distribution in the target.

At energy $\varepsilon_\nu=0.7$ GeV the RDWIA cross sections, in the maximum, are lower, than the PWIA and RFGM results, and this difference decreases with increasing energy transfer. At energy 2.5

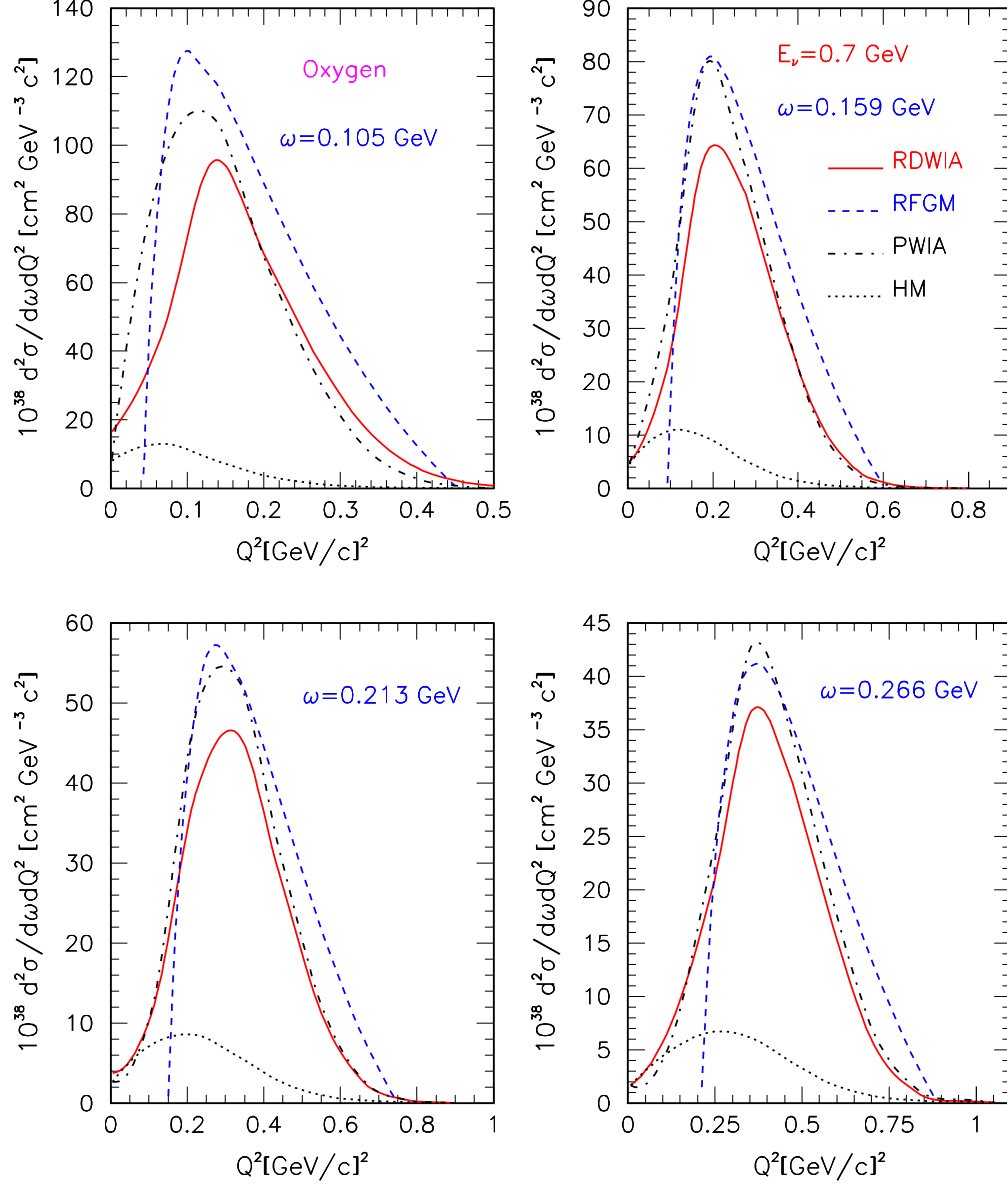


FIG. 1: (Color online) Inclusive cross section versus the four-momentum transfer Q^2 for neutrino scattering off ^{16}O with energy $E_\nu = 0.7 \text{ GeV}$ and for four values of energy transfer: $\omega = 0.105, 0.159, 0.213$ and 0.266 GeV . The solid line is the RDWIA calculation, whereas the dashed and dash-dotted lines are, respectively, the RFGM and PWIA calculations. The dotted line is the high-momentum component contribution to the inclusive cross section.

GeV, in the range of $\omega \geq 0.5 \text{ GeV}$, around the peak, the RFGM results are lower, than the RDWIA ones and fall down rapidly as Q^2 decreases. This trend is characteristic of the nucleon momentum distribution and the Pauli blocking effect as calculated in the Fermi gas model. On the contrary, the Q^2 -dependence of the RDWIA and PWIA cross sections at low Q^2 is softer due

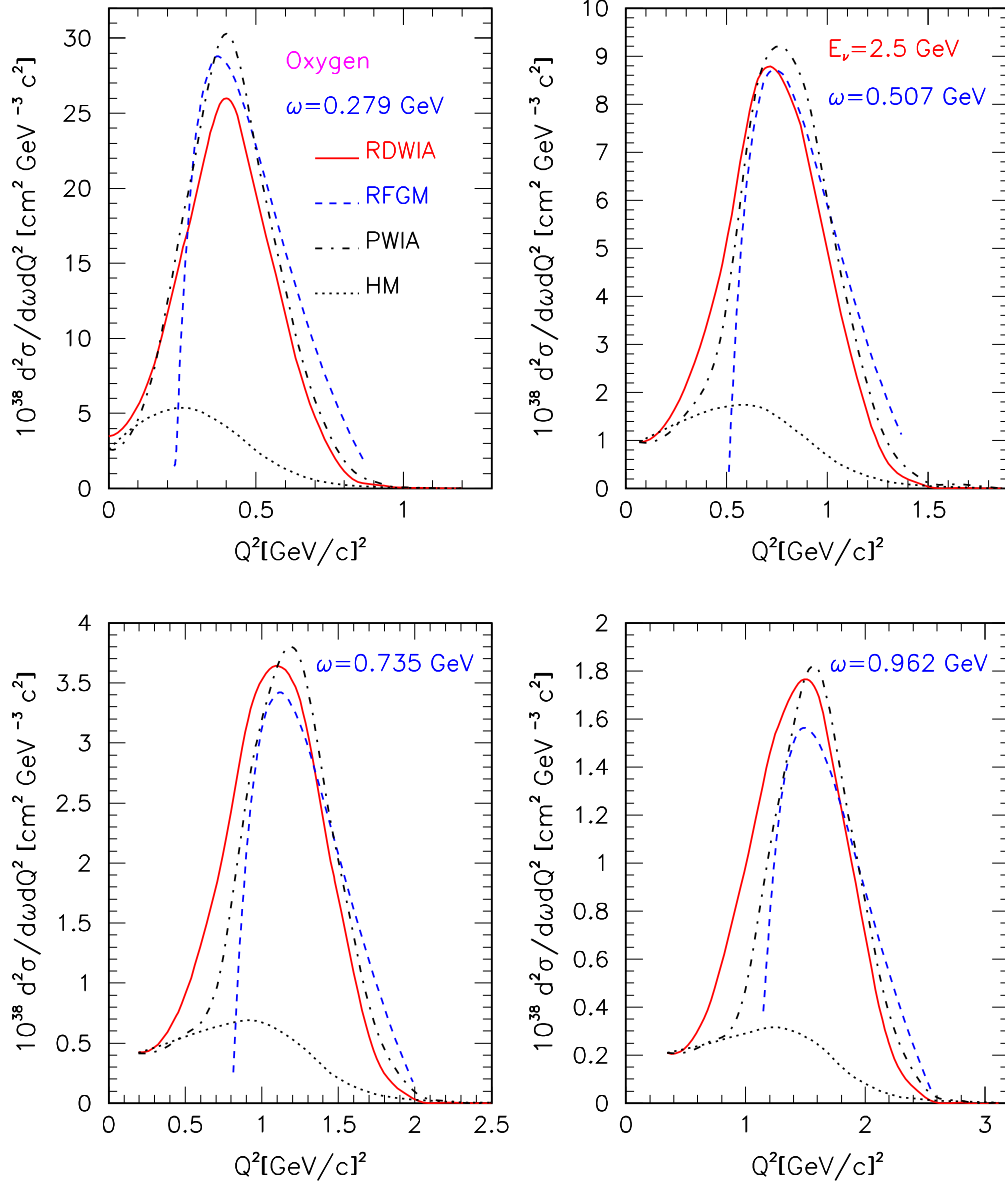


FIG. 2: (Color online) Same as Fig.1, but for the neutrino energy $\varepsilon_\nu=2.5$ GeV and for four values of energy transfer: $\omega=0.279, 0.507, 0.735$ and 0.962 GeV.

to the HM-component contribution, which becomes dominant at $Q^2 < 0.1$ (GeV/c) 2 .

Generally, theoretical uncertainties of the correlated NN-pairs contribution to the inclusive cross sections are higher as compared to the shell-nucleons contribution. The electron-nucleus scattering data [14, 32, 33] show that more complicated configurations, than a simple hard interaction between two nucleons, are involved in this case. Moreover, the off-shell ambiguities will be important for the high-momentum component, and one might expect the details of the off-shell extrapolation to

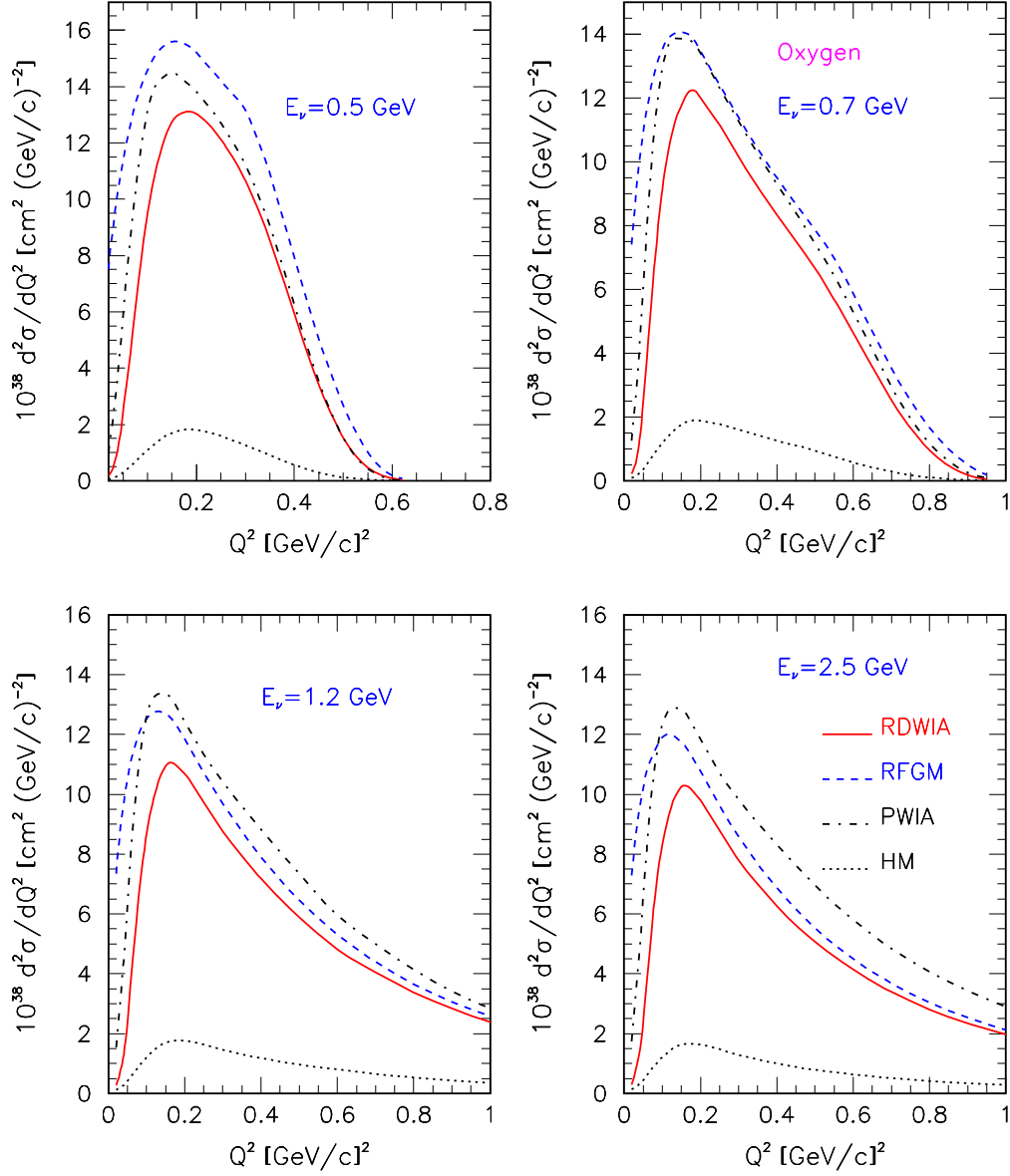


FIG. 3: (Color online) Inclusive cross section versus the four-momentum transfer Q^2 for neutrino scattering off ^{16}O and for four values of incoming neutrino energy: $\varepsilon_\nu=0.5, 0.7, 1.2$ and 2.5 GeV. The solid line is the RDWIA calculation, whereas the dashed and dash-dotted lines are, respectively, the RFGM and PWIA calculations. The dotted line is the high-momentum component contribution to the inclusive cross section.

become critical [34].

The inclusive cross sections for energies $\varepsilon_\nu=0.5, 0.7, 1.2$, and 2.5 GeV are presented in Fig.3, which shows $d^2\sigma/Q^2$ as a function of Q^2 . Here the results, obtained in the RDWIA, are compared with cross sections calculated in the PWIA and RFGM. The contributions of the NN-correlations

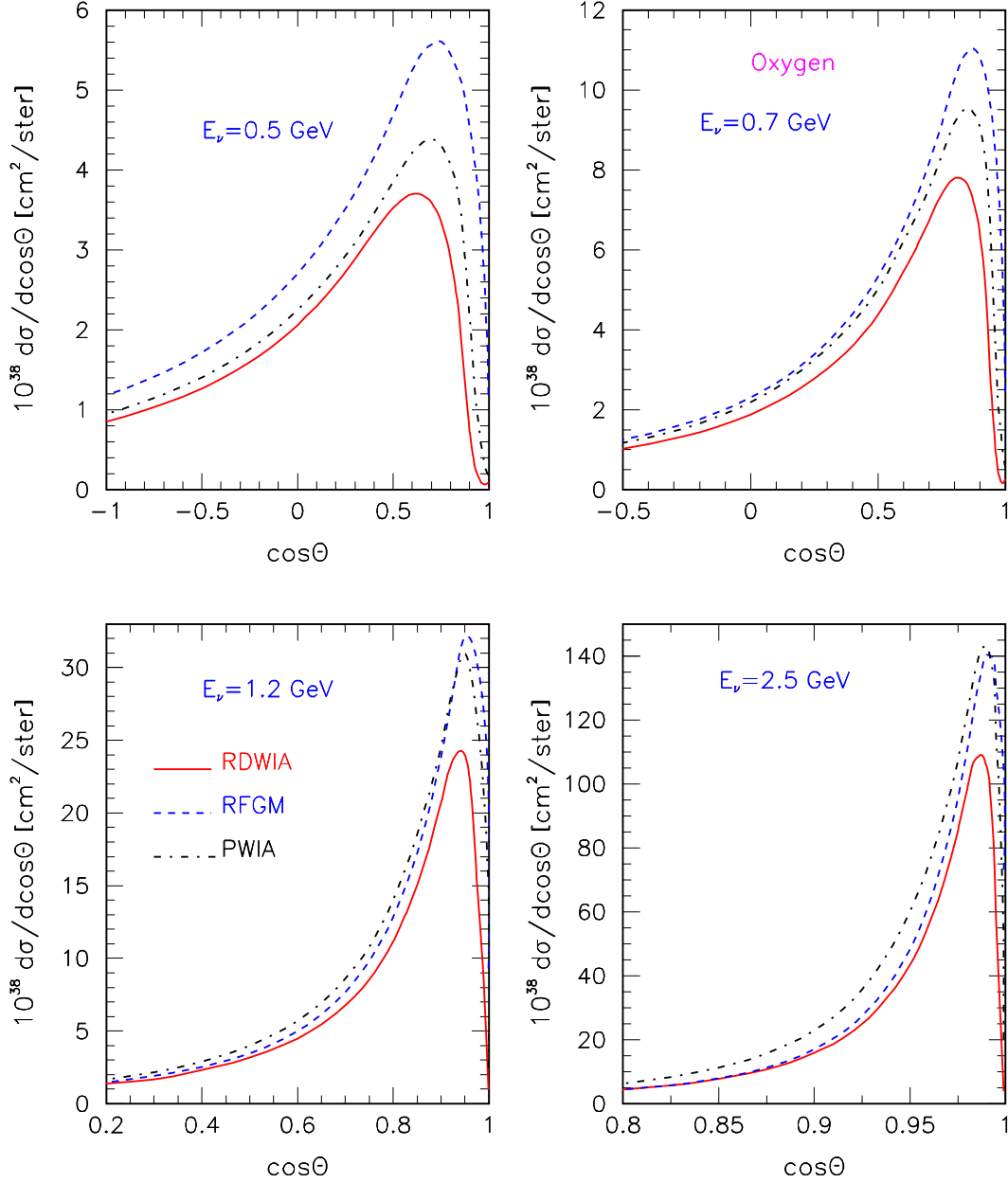


FIG. 4: (Color online) Inclusive cross section versus the muon scattering angle for four values of incoming neutrino energy: $\varepsilon_\nu=0.5, 0.7, 1.2$ and 2.5 GeV. The solid line is the RDWIA calculation, whereas the dashed and dash-dotted lines are, respectively, the RFGM and PWIA calculations.

are shown as well. The cross sections, calculated in the Fermi gas model, are higher, than those obtained within the RDWIA, and this difference increases with decreasing Q^2 . At $Q^2=0.1$ (GeV/c)² this discrepancy equals 54% for $\varepsilon_\nu=0.5$ GeV and 43% for $\varepsilon_\nu=2.5$ GeV. In the region around the maximum $Q^2=0.2$ (GeV/c)² the difference is about $\sim 18\%$ for $\varepsilon_\nu=0.5$ GeV and $\sim 11\%$ for $\varepsilon_\nu=2.5$

GeV. At $Q^2=0.05$ (GeV/c)² the contribution of the HM-component increases with energy from $\sim 15\%$ up to 23% in the energy range of $0.5 \div 2.5$ GeV.

Figure 4 shows the inclusive cross sections $d\sigma/d\cos\theta$ calculated in the RDWIA, PWIA, and RFGM approaches for energies $\varepsilon_\nu=0.5, 0.7, 1.2$, and 2.5 GeV. They are displayed as a function of $\cos\theta$. It is clear that in the region $0.8 < \cos\theta < 1$ the values of the RFGM cross sections are higher, than those obtained within the RDWIA, and this difference decreases with neutrino energy. For energy $\varepsilon_\nu=0.5$ GeV ($\varepsilon_\nu=2.5$ GeV) this discrepancy is about 25 times ($\sim 11\%$) at $\cos\theta=0.95$ and $\sim 89\%$ ($\sim 2\%$) at $\cos\theta=0.8$. We note that measured Q^2 and $\cos\theta$ -distributions of the CCQE events [2, 11, 12] show similar features as compared to the RFGM prediction.

Figures 5 and 6 show $\cos\theta_{pq}^m$ as a function of Q^2 calculated within the RDWIA and Fermi gas model kinematics for energies $\varepsilon_\nu=0.5$ and 2.5 GeV. The outgoing proton carries the kinematic energy, that is approximately ω . So far as ω is low, the problem consists in identifying the events with very soft recoil proton; for high ω this proton has high energy and may interact in the detector, making particle identification and track reconstruction more challenging. In these figures we show the contours of the phase volume in the $(\cos\theta_{pq}, Q^2)$ coordinates for $0.25 \leq \omega \leq 1$ GeV. Apparently, in the RDWIA kinematics this volume is larger, than in the RFGM. On the other hand, the difference decreases with ω and neutrino energy. Thus, systematic errors for the efficiency and purity of the two-track events selection are nuclear-model dependent.

We have studied the accuracy of the neutrino energy reconstruction with neglecting the systematics related to the event selection and resolution, i.e. with no detector effects or background. The study was performed with the values of cuts $(k_f)_{cut}=0.2$ GeV/c and $(\cos\theta)_{cut}=0$.

In Fig.7 the uncertainties of the energy reconstruction using Eq.(39) within the RDWIA and RFGM approaches are presented as functions of neutrino energy. The top panel shows the bias $\Delta = (\varepsilon_i - \varepsilon_r)/\varepsilon_i$, the middle panel shows the variance σ/ε_i (the energy resolution), and the efficiency of the one-track events detection is displayed in the bottom panel. It is clear that in the case of the Fermi gas model Eq.(39) systematically underestimates the neutrino energy and Δ decreases as the energy increases from -4.7% for $\varepsilon_\nu=0.3$ GeV up to -0.7% for $\varepsilon_\nu=2.5$ GeV. The variance σ/ε_i (efficiency) increases with energy from $\sim 5.4\%$ ($\sim 71\%$) up to $\sim 12\%$ ($\sim 99\%$) over the range of energy from 0.3 to 2.5 GeV.

In the RDWIA approach $\Delta \approx -5.2\%$ for $\varepsilon_\nu=0.3$ GeV and $\Delta \approx 3.9\%$ for $\varepsilon_\nu=1.6$ GeV. At energies $\varepsilon_\nu > 1.6$ GeV and at fixed values of cuts the denominator in Eq.(39) can be negative in the detection volume of the $(k_f, \cos\theta)$ phase space, which is determined by Eqs.(50) and (51). We note that the size of this volume decreases as $(\cos\theta)_{cut}$ increases. The energy resolution is about 8.3% for

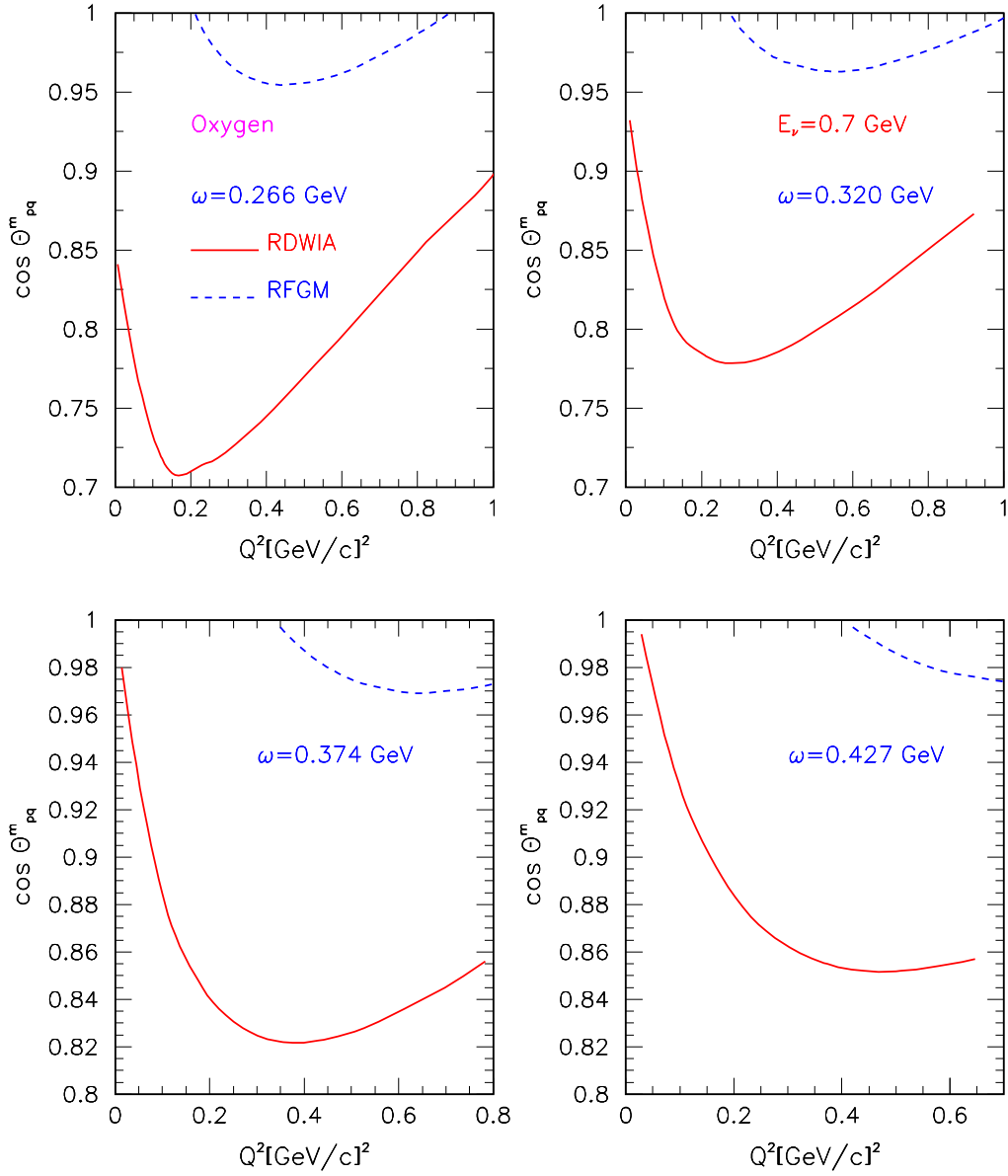


FIG. 5: (Color online) Contours of the phase volume in the $(\cos \theta_{pq}, Q^2)$ coordinates for neutrino scattering off ^{16}O with energy $\varepsilon_\nu = 0.7$ GeV and for four values of energy transfer: $\omega = 0.288, 0.320, 0.374$ and 0.427 GeV. The solid line is the RDWIA calculation, whereas the dashed line is the RFGM calculation.

$\varepsilon_\nu = 0.3$ GeV and $\sim 12.7\%$ for $\varepsilon_\nu = 1.6$ GeV, and the maximum of 15.4% is located around $\varepsilon_\nu = 0.8$ GeV. The efficiency rapidly increases with energy from 28% for $\varepsilon_\nu = 0.3$ GeV up to 96% for $\varepsilon_\nu = 1.6$ GeV. So, the values of the bias and energy resolution, obtained within the RDWIA, are higher, than those obtained in the Fermi gas model.

The accuracy of the mean energy method, which takes into account the nucleon momentum

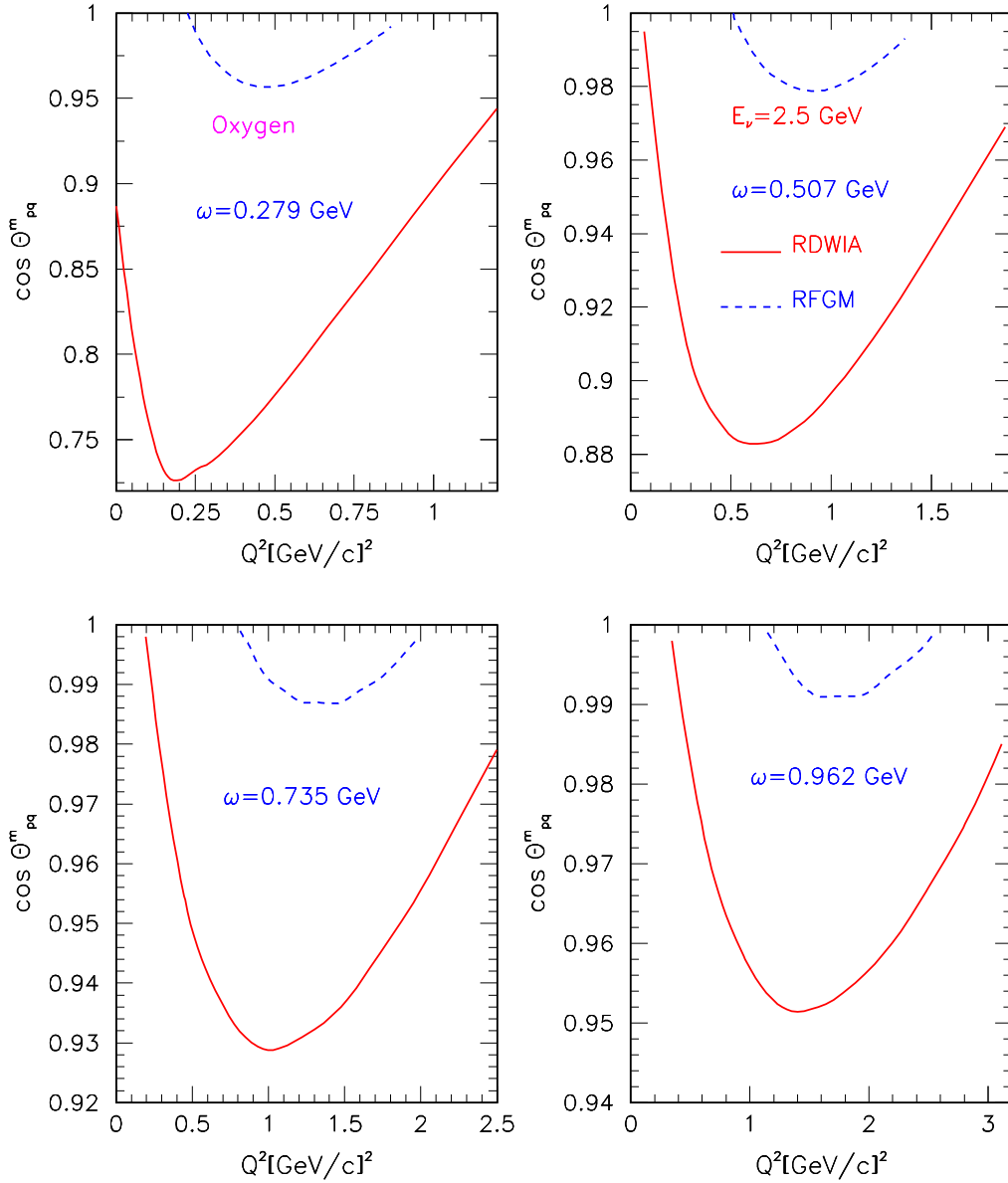


FIG. 6: (Color online) Same as Fig.5, but for neutrino energy $\varepsilon_\nu=2.5$ GeV and for four values of energy transfer: $\omega=0.279, 0.507, 0.735$ and 0.962 GeV.

distribution in the target, is shown in Fig.8. We assume that the maximum neutrino energy in the neutrino beam (Eq.(B8)) is $E_{max}=10$ GeV. The top and bottom panels show the biases and energy resolutions calculated within the RDWIA and RFGM. In the case of the RFGM the mean energy method systematically overestimates the neutrino energy; $\Delta=4.3\%$ for $\varepsilon_\nu=0.3$ GeV, $\Delta \approx 6\%$ for $\varepsilon_\nu=0.8$ GeV and decreases down to 3% for $\varepsilon_\nu=2.5$ GeV. The energy resolution increases with energy from 4.6% up to 11% in this energy range. In the RDWIA approach $\Delta \approx -4\%$, $(\sigma/\varepsilon_i) \approx 14\%$

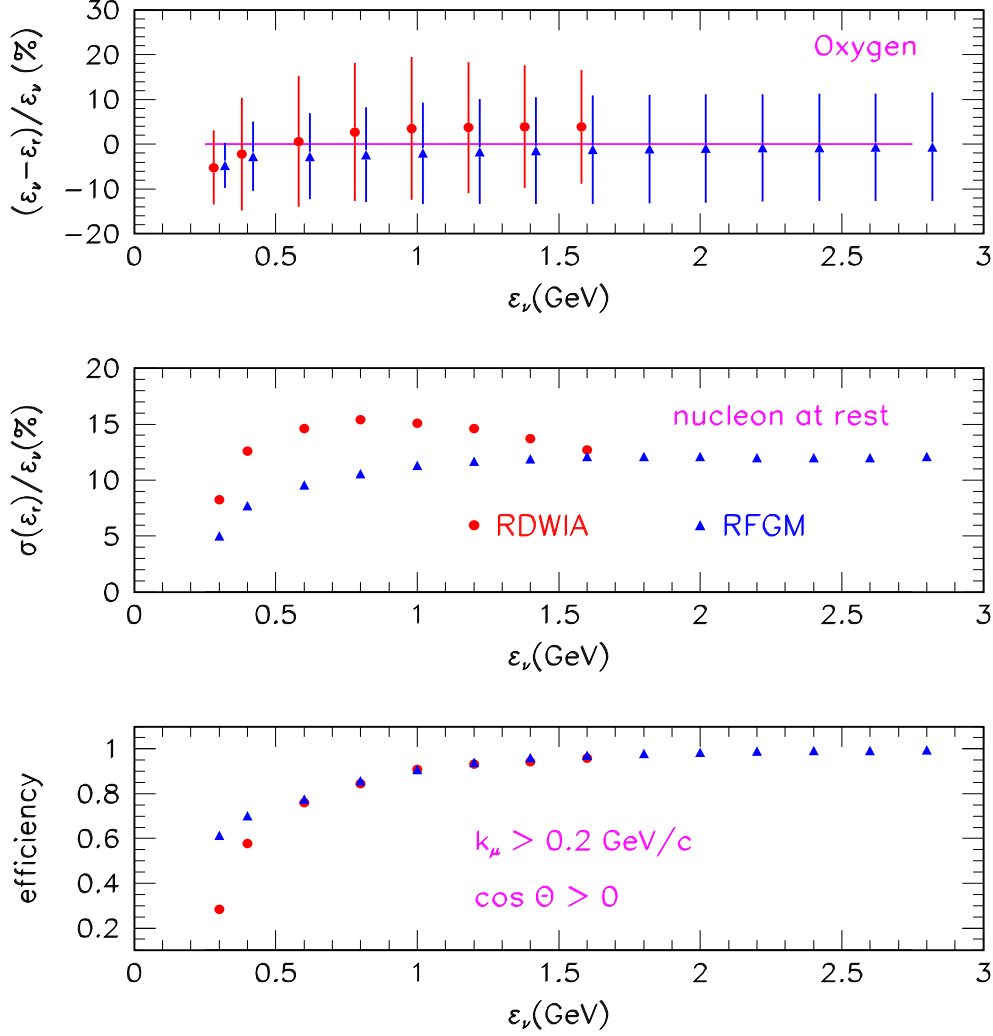


FIG. 7: (Color online) Bias (top panel), variance (middle panel) of the reconstructed neutrino energy, and the efficiency (bottom panel) of the one-track events detection with $k_f \geq 0.2$ (GeV/c) and $\cos \theta \geq 0$ as functions of neutrino energy. The neutrino energy reconstruction was formed assuming the target nucleon to be at rest inside the nucleus. The vertical bars show $\sigma[(\varepsilon_i - \varepsilon_r)/\varepsilon_i]$. As displayed in the key, the biases, variances and efficiencies were calculated in the RDWIA and RFGM.

for $\varepsilon_\nu = 0.3$ GeV, and $\Delta \approx 4.5\%$, $(\sigma/\varepsilon_i) \approx 10.5\%$ for $\varepsilon_\nu = 2.5$ GeV. It should be noted here that bias may depend on the value of E_{max} .

The effect of the nucleon momentum distribution in the target is shown in Fig.9. The biases, calculated within the RDWIA (top panel) and RFGM (bottom panel) using Eq.(39) (Δ_{fr}) and

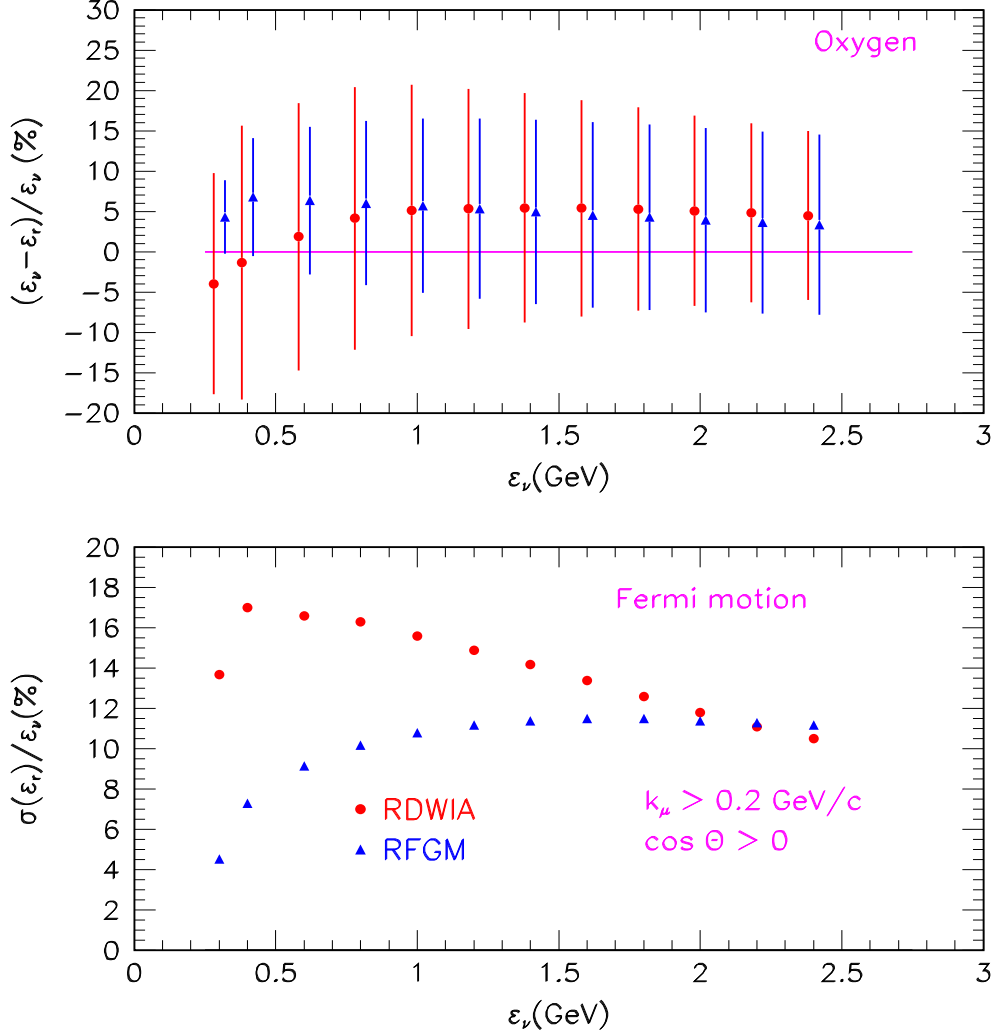


FIG. 8: (Color online) Bias (top panel) and variance (bottom panel) of the reconstructed neutrino energy as functions of neutrino energy. The energy reconstruction was formed taking into account the nucleon momentum distribution in the target. The vertical bars are the same as in Fig.7. As displayed in the key, the biases and variances were calculated in the RDWIA and RFGM.

the mean energy method (Δ_{me}), are presented as functions of neutrino energy. In the RDWIA approach the Δ_{fr} and Δ_{me} show similar behavior with neutrino energy, and the nucleon Fermi motion effect leads to increasing the bias by about 1.2%. In the Fermi gas model with this effect ε_r is overestimated, and $\Delta_{fr}(\Delta_{me}) = -4.7\%(4.3\%)$ for energy 0.3 GeV and $\Delta_{fr}(\Delta_{me}) = -0.7\%(3.4\%)$ for $\varepsilon_\nu = 2.5$ GeV.

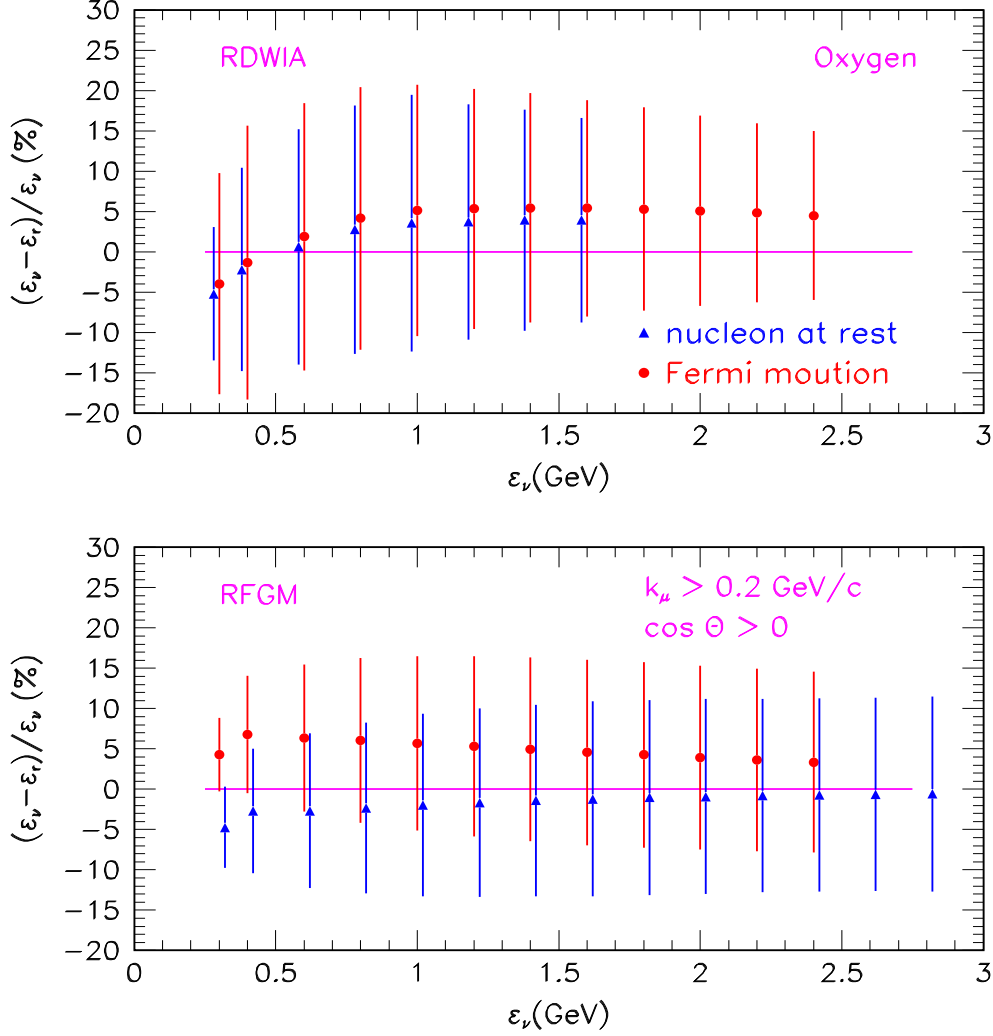


FIG. 9: (Color online) Biases calculated in the RDWIA (top panel) and RFGM (bottom panel) as functions of neutrino energy. The vertical bars are the same as in Fig.7. As displayed in the key, the energy reconstructions were formed with and without the nucleon momentum distribution.

Apparently, the accuracy of the kinematic reconstruction of neutrino energy for one-track events depends on the nuclear models of QE neutrino CC interaction with nuclei and on the neutrino energy reconstruction methods. In the K2K and MiniBooNE experiments Eq.(39) is applied for the energy reconstruction. The bias Δ_{FG} and energy resolution $\delta_{FG} = (\sigma/\epsilon_i)_{FG}$ were calculated using MC simulation based on the Fermi gas model. We can estimate the

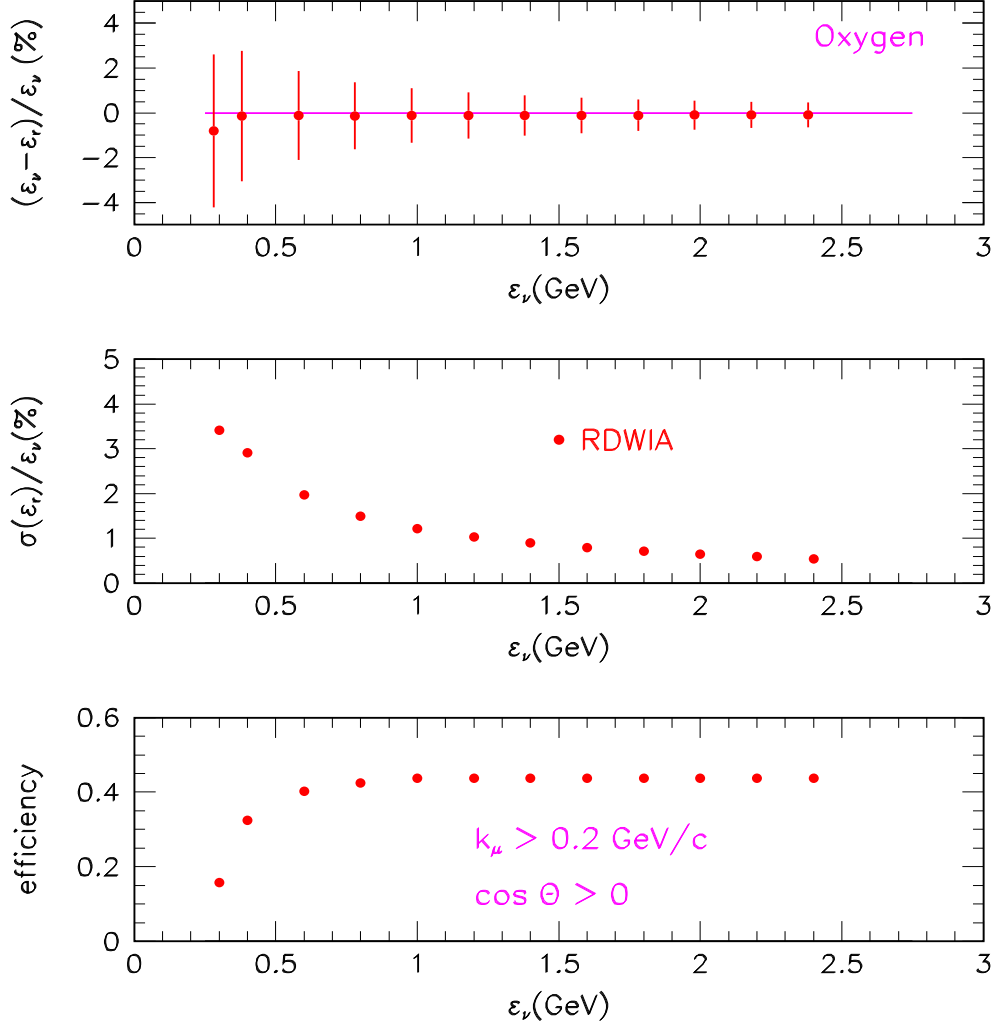


FIG. 10: (Color online) Bias (top panel), variance (middle panel) of the reconstructed neutrino energy, and the efficiency (bottom panel) of the two-track events detection with $k_f \geq 0.2$ (GeV/c) and $\cos \theta \geq 0$. The vertical bars are the same as in Fig.7. The bias, variance and efficiencies were calculated within the RDWIA.

systematic uncertainties of this approach by comparing Δ_{FG} and δ_{FG} with Δ_R and δ_R evaluated in the RWDIA approach using the mean energy method. It is clear that uncertainties depend on neutrino energy: $\Delta_{FG}(\Delta_R) \approx -4.7\%(-4\%)$ and $\delta_{FG}(\delta_R) \approx 5.4\%(13.7\%)$ for $\varepsilon_\nu = 0.3$ GeV; $\Delta_{FG}(\Delta_R) \approx -2.3\%(4.1\%)$ and $\delta_{FG}(\delta_R) \approx 10.6\%(16.3\%)$ for $\varepsilon_\nu = 0.8$ GeV; $\Delta_{FG}(\Delta_R) \approx -0.7\%(4.5\%)$ and $\delta_{FG}(\delta_R) \approx 12\%(11.5\%)$ for $\varepsilon_\nu = 2.5$ GeV. So, the bias uncertainty increases with

energy from $(\Delta_R - \Delta_{FG}) \approx 0.7\%$ for $\varepsilon_\nu = 0.3$ GeV up to 5.2% for $\varepsilon_\nu = 2.5$ GeV, and the energy resolution uncertainty decreases with increasing energy from $\delta_R - \delta_{FG} \approx 8.3\%$ down to 0.5% in this energy range. We note that these estimations may depend on the values of $(k_f)_{cut}$, $(\cos \theta)_{cut}$ and E_{max} .

In Fig.10 the accuracy of the energy reconstruction for the two-track events, calculated using Eq.(55) within the RDWIA, is shown as a function of neutrino energy. The top panel shows the bias, the middle panel shows the variance, and the bottom panel shows the efficiency of the two-track events detection with cuts $k_f \geq 0.2$ GeV/c and $\cos \theta \geq 0$ for muon tracks and without any cuts for the proton tracks. At energy $\varepsilon_\nu > 0.3$ GeV the bias is $\Delta \approx -0.1\%$ and does not depend on the neutrino energy. The energy resolution decreases as the energy increases from 3.4% for $\varepsilon_\nu = 0.3$ GeV up to 0.5% for $\varepsilon_\nu = 2.5$ GeV, and the efficiency rapidly increases with energy from $\sim 16\%$ up to $\sim 44\%$ in this energy range. These estimations show that the accuracy of the calorimetric method can be higher, than the kinematic one and does not depend on the model of CC neutrino QE interaction with nuclei and on the nucleon momentum distribution in the target. The challenge is identifying the proton track and reconstructing its kinetic energy with reliable accuracy at the low threshold energy for proton detection.

V. CONCLUSIONS

In this paper, we study the quasi-elastic neutrino charged-current scattering on the oxygen target in various approximations (PWIA, RDWIA, RFGM) making particular emphasis on the nuclear-model dependence of the results. In the RDWIA, the LEA program, adapted to neutrino interactions, was used for calculating the differential cross sections with the effect of NN-correlations in the target ground state.

The inclusive $d^2\sigma/dQ^2$ and $d\sigma/d\cos \theta$ cross sections, calculated within the RDWIA, and the measured Q^2 , $\cos \theta$ -distributions of CCQE events exhibit similar feature as compared to the Fermi gas model. The magnitude of inclusive cross sections $d^2\sigma/dQ^2$ and $d\sigma/d\cos \theta$ is lower in the RDWIA calculations, than that of the Fermi gas model, and in the region around the maximum $Q^2 = 0.2$ (GeV/c) 2 the difference is about 18% for $\varepsilon_\nu = 0.5$ GeV and 11% for $\varepsilon_\nu = 2.5$ GeV. The contribution of the HM-component at $Q^2 = 0.05$ (GeV/c) 2 increases with neutrino energy from 15% up to 23% in this energy range. Note that the measured Q^2 and $\cos \theta$ -distributions of CCQE events are also lower, than the RFGM prediction at low Q^2 .

We have shown that the efficiency and purity of the CCQE two-track events selection are nuclear-

model dependent, and the difference decreases with increasing energy transfer and neutrino energy.

We have studied the nuclear-model dependence of the energy reconstruction accuracy, neglecting the systematics related to event selection and resolution. We found that the accuracy of the kinematic reconstruction for one-track events depends on the nuclear model of CCQE neutrino interaction and on the neutrino energy reconstruction method. The uncertainties in the reconstructed energy bias increase in the energy range of $0.3 \div 2.5$ GeV from $\sim 0.7\%$ up to 5.4% , and the energy resolution ambiguities decrease from 8.3% down to 0.5% with increasing energy. In the case of two-track events the accuracy may be higher and does not depend on the nuclear models of CCQE neutrino-nucleus interaction.

We conclude that the use of RDWIA in the Monte Carlo simulation of neutrino detector and the data analysis would allow one to reduce the systematic uncertainty in neutrino oscillation parameters.

Acknowledgments

The author greatly acknowledges S. Kulagin, S. Mikheyev, J. Morfin, G. Zeller, and R. Gran for fruitful discussions at different stages of this work.

APPENDIX A: EQUATION FOR NEUTRINO ENERGY

In Eq.(43)

$$A\varepsilon_r^2 - B\varepsilon_r + C = 0.$$

the coefficients A, B, and C are defined as follows:

$$A = a^2 - \mathbf{p}_m^2 z^2, \tag{A1a}$$

$$B = ab - 2\mathbf{p}_m^2 z^2 k_f \cos \theta, \tag{A1b}$$

$$C = b^2/4 - \mathbf{p}_m^2 z^2 k_f^2, \tag{A1c}$$

where

$$a = \varepsilon_{ef} - k_f \cos \theta, \tag{A2a}$$

$$b = \varepsilon_{ef}^2 - (|\mathbf{p}_m|^2 + m^2) - k_f^2, \tag{A2b}$$

$$z = \cos \tau = \mathbf{p}_m \cdot \mathbf{q} / |\mathbf{p}_m \cdot \mathbf{q}|. \tag{A2c}$$

In the Fermi gas model

$$\varepsilon_{ef} = \varepsilon_f - \sqrt{\mathbf{p}_m^2 + m^2} + \epsilon_b, \quad (\text{A3})$$

in the RDWIA model, for shell-nucleons

$$\varepsilon_{ef} = \varepsilon_f - m_A + [(m_A - m + \varepsilon_m)^2 + \mathbf{p}_m^2]^{1/2}, \quad (\text{A4})$$

and for nucleons in the correlated NN-pair

$$\varepsilon_{ef} = \varepsilon_f - \varepsilon_N. \quad (\text{A5})$$

APPENDIX B: MOMENTS OF RECONSTRUCTED NEUTRINO ENERGY

In the Fermi gas model with the p.d.f.

$$S(\mathbf{p}_m, \varepsilon_m) = \frac{3}{4\pi p_F^3} \delta(\varepsilon_m - \epsilon_b) \quad (\text{B1})$$

Eq.(45) takes the form

$$\langle \varepsilon_r^n(k_f, \cos \theta) \rangle = \frac{3}{4\pi p_F^3} \int_{p_{min}}^{p_{max}} p^2 dp \int_{z_{min}}^{z_{max}} [\varepsilon_r(k_f, \cos \theta, p, z)]^n dz, \quad (\text{B2})$$

where $z = \cos \tau$ and ε_r is given by Eqs.(44), (A1), (A2), and (A3). In the RDWIA the p.d.f. can be written as follows:

$$S(\mathbf{p}, \varepsilon) = \sum_{\alpha} v_{\alpha} S_{\alpha}(\mathbf{p}) \delta[\varepsilon - (\varepsilon_m)_{\alpha}] + v_{NN} S_{NN}(\mathbf{p}, \varepsilon) \quad (\text{B3})$$

and we have

$$\langle \varepsilon_r^n(k_f, \cos \theta) \rangle = \sum_{\alpha} v_{\alpha} \langle \varepsilon_{r,\alpha}^n(k_f, \cos \theta) \rangle + v_{NN} \langle \varepsilon_{r,NN}(k_f, \cos \theta) \rangle, \quad (\text{B4a})$$

$$\langle \varepsilon_{r,\alpha}^n(k_f, \cos \theta) \rangle = \int_{p_{min}}^{p_{max}} p^2 dp \int_{z_{min}}^{z_{max}} S_{\alpha}(\mathbf{p}) [\varepsilon_{r,\alpha}(k_f, \cos \theta, p, z)]^n dz, \quad (\text{B4b})$$

$$\langle \varepsilon_{r,NN}^n(k_f, \cos \theta) \rangle = \int_{p_{min}}^{p_{max}} p^2 dp \int_{\varepsilon_{min}}^{\varepsilon_{max}} d\varepsilon \int_{z_{min}}^{z_{max}} S_{NN}(\mathbf{p}, \varepsilon) [\varepsilon_{r,NN}(k_f, \cos \theta, p, \varepsilon, z)]^n dz, \quad (\text{B4c})$$

where S_{α} and S_{NN} are, respectively, the p.d.f. for the momentum and energy of nucleons on the shell α and in the correlated NN-pairs, $\varepsilon_{r,\alpha}^n$ and $\varepsilon_{r,NN}^n$ are given by Eqs.(44), (A1), (A2), (A4), (A5) and the sum is taken over occupied shells. The coefficients v_{α} and v_{NN} are

$$v_{\alpha,NN} = \frac{1}{\sigma_{\alpha,NN}} \left(\frac{d^2 \sigma}{dk_f d \cos \theta} \right)_{\alpha,NN}, \quad (\text{B5})$$

where

$$\sigma_{\alpha,NN} = \int \left(\frac{d^2\sigma}{dk_f d\cos\theta} \right)_{\alpha,NN} dk_f d\cos\theta \quad (\text{B6})$$

The integral is calculated with $(k_f)_{min} = (k_f)_{cut}$ and $(\cos\theta)_{min} = (\cos\theta)_{cut}$. Using Eqs.(47), (B4), we have

$$\langle \varepsilon_r^n(\varepsilon_i) \rangle = \sum_{\alpha} w_{\alpha} \langle \varepsilon_r^n(\varepsilon_i) \rangle_{\alpha} + w_{NN} \langle \varepsilon_r^n(\varepsilon_i) \rangle_{NN}, \quad (\text{B7})$$

where $w_{\alpha,NN} = \sigma_{\alpha,NN} / (\sum_{\alpha} \sigma_{\alpha} + \sigma_{NN})$. In Eqs.(B2) and (B4) the limits of integration over z are: $z_{min}=-1$ and $z_{max}=\min\{1, z_l\}$. The value of z_l is obtained from the requirement $\varepsilon_r(k_f, \cos\theta) \leq E_{max}$, where E_{max} is the maximum neutrino energy in the neutrino beam. We note that this constrain on z_{max} leads to increasing bias Δ in the reconstructed energy. Then from Eqs.(36a), (40), (41), and (42) with $\varepsilon_i = E_{max}$ it follows, that

$$z_l = \frac{(\omega_{max} + \epsilon)^2 - (\mathbf{p}_m^2 + \mathbf{q}^2 + m^2)}{2|\mathbf{p}_m||\mathbf{q}|}, \quad (\text{B8})$$

where $\omega_{max} = E_{max} - \varepsilon_f$ and $\mathbf{q}^2 = E_{max}^2 + k_f^2 - 2E_{max}k_f \cos\theta$. In the Fermi gas model $\epsilon = \sqrt{\mathbf{p}_m^2 + m^2} - \epsilon_b$, in the RDWIA for scattering off shell-nucleons $\epsilon = m_A - \sqrt{\mathbf{p}_m^2 + m_B^2}$, and $\epsilon = \varepsilon_N$ for scattering off nucleons in the correlated NN-pair.

For the two-track events the moments of the $\varepsilon_r(k_f, \cos\theta)$ distribution can be written as

$$\langle \varepsilon_r^n(\varepsilon_i) \rangle = \sum_{\alpha} w_{\alpha} \langle \varepsilon_r^n(\varepsilon_i) \rangle_{\alpha}, \quad (\text{B9})$$

where

$$\langle \varepsilon_r^n(\varepsilon_i) \rangle = \int dk_f \int d\cos\theta \int_0^{2\pi} d\phi \int_{p_{min}}^{p_{max}} [\varepsilon_f + T_p + \langle \varepsilon_m \rangle]^n W_{\alpha}(k_f, \cos\theta, \phi, p_m) dp_m, \quad (\text{B10a})$$

$$W_{\alpha} = \frac{1}{\sigma_{\alpha}^{ex}} \left[\frac{d^5\sigma}{dk_f d\cos\theta d\phi dp_m} \right]_{\alpha} \quad (\text{B10b})$$

$$\sigma_{\alpha}^{ex} = \int dk_f \int d\cos\theta \int_0^{2\pi} d\phi \int_{p_{min}}^{p_{max}} \left[\frac{d^5\sigma}{dk_f d\cos\theta d\phi dp_m} \right]_{\alpha} dp_m, \quad (\text{B10c})$$

$$w_{\alpha} = \sigma_{\alpha}^{ex} / \sum_{\alpha} \sigma_{\alpha}^{ex} \quad (\text{B10d})$$

and $d^5\sigma/dk_f d\cos\theta d\phi dp_m$ is the QE neutrino CC scattering exclusive cross section (10) in terms of a missed momentum p_m .

- [2] A. A. Aguilar-Arevalo *et al.*, (The MiniBooNE Collaboration), Phys. Rev. Lett. **100**, 032301, 2008
- [3] P. Adamson *et al.*, (MINOS Collaboration), Phys. Rev. Lett. **97**, 191801, 2006
- [4] K. S. McFarland *et al.*, (MiNERvA Collaboration), Nucl. Phys. Proc. Suppl. **159**, 107, 2006.
- [5] T. Nakadaira *et al.*, (T2K Collaboration), Nucl. Phys. Proc. Suppl. **149**, 303, 2006.
- [6] G. Rosa *et al.*, (OPERA Collaboration), Nucl. Phys. Proc. Suppl. **145**, 98, 2005.
- [7] D. S. Ayres *et al.*, (NOvA Collaboration), arXiv:hep-ex/0503053.
- [8] G. P. Zeller, arXiv:hep-ex/0312061.
- [9] R. A. Smith and E. J. Moniz, Nucl. Phys. **B43**, 605, 1972; *erratum: ibid.* **B101**, 547, 1975
- [10] A. V. Butkevich and S. P. Mikheyev, Phys. Rev. **C72**, 025501, 2005.
- [11] R. Gran *et al.*, (K2K Collaboration), Phys. Rev. **D74**, 052002, 2006.
- [12] T. Katori *et al.*, (MiniBooNE Collaboration), AIP. Conf. Proc. **967**, 123, 2007.
- [13] A. V. Butkevich and S. A. Kulagin, Phys. Rev. **C76**, 045502, 2007.
- [14] K. G. Fissum *et al.*, Phys. Rev. **C70**, 034606, 2004
- [15] A. Meucci, C. Giusti, and F. D. Pacati, Nucl. Phys. **A739**, 277, 2004.
- [16] C. Maieron, M. C. Martinez, J. A. Caballero, and J. M. Udias, Phys. Rev. **C68**, 048501, 2003.
- [17] M. C. Martinez, P. Lava, N. Jachowicz, J. Ryckebusch, K. Vantournhout, and J. M. Udias, Phys. Rev. **C73**, 024607, 2006.
- [18] T. de Forest, Nucl. Phys. **A392**, 232, 1983.
- [19] P. Mergell, U.-G. Meissner, and D. Drechsel, Nucl. Phys. **A596**, 367, 1996.
- [20] B. Serot, J. Walecka, Adv. Nucl. Phys. **A16**, 1, 1986.
- [21] M. M. Sharma, M. A. Nagarajan, and P. Ring, Phys. Lett. **B312**, 377, 1993.
- [22] M. Leuschner *et al.*, Phys. Rev. **C49**, 955, 1994
- [23] J. M. Udias, P. Sarriguren, E. Moya de Guerra, E. Garrido, and J. A. Caballero, Phys. Rev. **C51**, 3246, 1995.
- [24] M. Hedayati-Poor, J. I. Johansson, and H. S. Sherif, Phys. Rev. **C51**, 2044, 1995.
- [25] J. J. Kelly, <http://www.physics.umd.edu/enp/jjkelly/LEA>
- [26] E. D. Cooper, S. Hama, B. C. Clark, and R. L. Mercer, Phys. Rev. **C47**, 297, 1993.
- [27] S. Frullani and J. Mougey, Adv. Nucl. Phys. **14**, 1, 1984.
- [28] C. Ciofi degli Atti and S. Simula, Phys. Rev. **C53**, 1689, 1996.
- [29] S. A. Kulagin and R. Petti, Nucl. Phys. **A765**, 126, 2006.
- [30] C. L. Smith, Phys. Rep. **3**, 261, 1972.
- [31] M. Hasegawa *et al.*, (K2K Collaboration), Phys. Rev. Lett. **95**, 252301, 2005
- [32] D. Rohe *et al.*, Nucl. Phys. Proc. Suppl. **159**, 152, 2006.
- [33] M. Iodice *et al.*, Phys. Lett. **B653**, 392, 2007
- [34] J. J. Kelly, Adv. Nucl. Phys. **23**, 75, 1996.